ADVANCES IN GEODESY AND GEOINFORMATION
(formerly GEODESY AND CARTOGRAPHY)
Vol. 75, no. 1, article no. e73, 2026

https://doi.org/10.24425/agg.2026.157429

Original paper

Flood identification in Jakarta (2018 and 2020): a combined InSAR coherence and rapid flood mapping

Lia Lidyani, Naufal Setiawan*

Universitas Pembangunan Nasional "Veteran" Yogyakarta, Yogyakarta, Indonesia
e-mail: lidyaniliaa@gmail.com; ORCID: http://orcid.org/0009-0008-4400-8211
e-mail: naufal.setiawan@upnyk.ac.id; ORCID: http://orcid.org/0000-0002-2350-4477

*Corresponding author: Naufal Setiawan, e-mail: naufal.setiawan@upnyk.ac.id

Received: 2025-08-16 / Accepted: 2025-11-16

Abstract: Jakarta has experienced a land subsidence rate of 3–10 cm per year, intensifying existing environmental pressures that gradually shape long-term hydrological responses in the region. Additionally, low infiltration factors, soil compaction, poor drainage systems, and rising sea levels resulted in an increase in the quantity of flooding in Jakarta, affecting the area of inundation, height of the floodwaters, and duration of flooding in the region. Consequently, flooding continued to recur during the rainy period with increasing severity. Based on these facts, efforts are needed to minimize or address the areas affected by flooding in Jakarta, one of which involves flood identification through the utilization of active remote sensing technology. We utilized Sentinel-1A to generate coherence values based on the Interferometric Synthetic Aperture Radar (InSAR) coherence method. Additionally, we applied Rapid Flood Mapping based on backscatter values. Our results indicate that the image acquisition period significantly dictates the outcomes, with the image pairs of "dry_rain" proving more effective than "rain_rain" in Jakarta's flood identification. Furthermore, integrating results from both methods improves flood identification, as they can validate each other. Specifically, the mapped flood extent was influenced by rainfall intensity and the spatial distribution of validation points within the presumed flood zones.

Keywords: flood, InSAR coherence, rapid flood mapping

1. Introduction

Population density compares the number of people and the area inhabited (Mantra, 2003). Of the 33 provinces in Indonesia, Jakarta Province ranks first with a density of 14,470 inhabitants per km^2, followed by West Java (1,217), Yogyakarta (1,104), Banten (1,100), Central Java (987), and East Java (784) (Kodoatie, 2013). In this case, the number and rate of urban population that tends to increase results in environmental degradation, and the existing infrastructure system becomes inadequate (Kodoatie, 2013). The increase in population, especially in Jakarta, has consequences in the form of excessive groundwater withdrawal, which has the potential to cause land subsidence (Abidin et al., 2015). Based on geodetic measurement methods such as Leveling, Global Navigation Satellite System (GNSS), and Interferometric Synthetic Aperture Radar (InSAR) surveys conducted from 1982 to 2014, Jakarta has a land subsidence rate of 3–10 cm per year with the information that along the coastal area of Jakarta has experienced a relatively greater decline than non-coastal areas (Abidin et al., 2015). In addition to water extraction factors, land subsidence is caused by the natural consolidation of alluvial soil and the burden on infrastructure and buildings (Abidin et al., 2015). These factors are exacerbated by the low infiltration rate, soil layers that experience compaction, poor drainage systems, and the phenomenon of sea level rise so that the quantity of flooding in Jakarta increases, both the area of inundation, the height of inundation, and the duration of flooding in the area (Pasaribu et al., 2015). Therefore, flood events in Jakarta will continue to recur during the rainy period with an increasing volume (Kodoatie, 2013).

On February 5 and 15, 2018, Jakarta experienced extreme flooding during the peak of the rainy season (Dwi and Nurhadi, 2022). The flood submerged some areas of East Jakarta, West Jakarta, North Jakarta, and Central Jakarta. According to data from the Jakarta Regional Disaster Management Agency (BPBD), 53 "Rukun Warga" (a neighborhood-level administrative unit in Indonesia) from 18 villages throughout Jakarta are flooded. As a result, 11.824 Jakarta residents had to evacuate. Moreover, from late 2019 to early 2020, Jakarta once again experienced extreme flooding. The Meteorology, Climatology, and Geophysics Agency (BMKG) noted that the flood occurred due to extreme rainfall reaching 377 mm. Consequently, a total of 24 victims died due to drifting, injured, and being stung by electric cables, more than 31.000 residents were displaced, and 724 areas were affected by power outages.

The severe consequences of the two flood periods highlight the importance of minimizing or overcoming flood-affected areas in Jakarta. Remote sensing is one of the technologies that can measure and monitor floods and provide wide coverage (Selmi et al., 2014). Optical remote sensing has been used for dynamic flood monitoring based on low water reflectance in the infrared band and high reflectance in the band blue/green (Twele et al., 2016). However, during flood events in urban areas, cloud cover due to rainfall limits the effectiveness of optical remote-sensing satellites for flood observation (Riyanto et al., 2022).

To address these limitations, Synthetic Aperture Radar (SAR) is a solution to map floods because they are not affected by the day or night, weather conditions, cloud cover, or fog, hindering vital information (Bioresita et al., 2022). The SAR produced monochromatic imagery containing reflectance information from the observation area by observing the difference in backscatter before and after the event to identify flooded areas (Ciecholewski, 2017); flood water can easily be differentiated due to the specular reflectance that occurs on the smooth surface of the water produces darker color on SAR backscattering on vacant land or areas which is rarely overgrown by plants (Chini et al., 2019; Bioresita et al., 2022). Therefore, the SAR backscattering does not accurately detect inundation in complex environments, such as vegetated and urban areas (Chini et al., 2019). Another challenge is the atmosphere, high rainfall, and strong winds, which cause rough surface and even detection errors due to reduced contrast between the backscatter of flooded and unflooded land (Pierdicca et al., 2018).

Building on these constraints, recent studies have explored improving the ability to detect and map floods in vegetated and urban areas using the Interferometric Synthetic Aperture Radar Coherence method (InSAR Coherence) (Santoro et al., 2007, [article73:43]2010; Brisco et al., 2017; Mohammadimanesh et al., 2018a, [article73:33]2018b; Canisius et al., 2019a; DeLancey et al., 2019; Tay et al., 2020; Cartus et al., 2022; Schumann et al., 2023; Garg et al., 2024). InSAR Coherence measures the stability and consistency of the phase relationships between two radar signals (Garg et al., 2024).

In this case, coherence before a flood plays a role in identifying the presence of vegetation. In this context, pre-flood coherence helps to identify vegetated areas. Meanwhile, post-flood coherence can distinguish between flooded and non-flooded vegetation on bare land, identify fields where water has receded or those experiencing prolonged inundation, and assess the persistence of floodwater in urban regions (Pulvirenti et al., 2016). In addition, low coherence allows the detection of floodwater. Conversely, a high coherence value enables the detection of changes in the water surface and flood volume that have been inundated for a long time (Pulvirenti et al., 2016). Therefore, the InSAR Coherence provided by Very High Resolution (VHR) SAR data shows the potential for more accurate flood mapping in urban areas and vegetation because ρ has a high sensitivity to well-documented surface changes and enables the detection of damage caused by catastrophic events such as volcanic eruptions, earthquakes, and floods (Chini et al., 2019). This method has been tested and can map flooding due to Hurricane Harvey in rural areas and built-up areas of Houston, Texas, United States, through research conducted by Chini et al. (2019).

Our novelty that differentiates it from Chini et al. (2019) research is integrating InSAR Coherence with the Rapid Flood Mapping (RFM) result to identify flood areas. RFM utilizes Sentinel-1A Ground Range Detected (GRD) images to derive backscatter (amplitude), enabling faster flood detection. Furthermore, we investigated the impact of periodic variation by comparing flood identification results using master images acquired during rainy and dry periods, revealing surface changes related to flooding. Generating detailed information about flood-prone areas is vital to increase public awareness, support institutional decision-making for flood disaster mitigation, and improve conditions in vulnerable regions. The following sections present the research problem, describe the materials and methods used, discuss the results, and conclude our study.

2. Motivation and study objective

This research was conducted because Jakarta is highly prone to flooding, especially during the rainy season, requiring innovative efforts to minimize and manage flood-affected areas. The study identifies and validates flood-prone zones in Jakarta using Sentinel-1A imagery through InSAR Coherence and Rapid Flood Mapping methods, which provide detailed information on vulnerable areas, enhance flood awareness, and support decision-making for mitigation and improvement efforts. The research aims to (1) analyze the effect of image period use on InSAR Coherence and Rapid Flood Mapping results to determine the most effective period for flood identification, (2) assess the integration of both methods in identifying floods, and (3) examine factors influencing the integration results in flood detection across Jakarta.

3. State of problems

Geographically, Jakarta is a low-lying area between the coast and the river's upper reaches, making it prone to frequent flooding. Three main factors cause this condition: (1) local flooding due to high-intensity and prolonged rainfall, which leads to excessive water volumes that can no longer be accommodated in waterways or low-lying (concave) areas; (2) flood discharge from upstream rivers in West Java and Banten, which must pass through Jakarta before reaching the sea; and (3) tidal flooding in Jakarta's coastal zones, which makes the area susceptible to flash floods. Thus, efforts are needed to reduce the flood impact in Jakarta. One such effort is flood identification using active remote sensing technology, namely, SAR.

Jakarta is an urban area with a high built-up area. Therefore, flood identification in Jakarta is challenging owing to the complexity of the urban environment, where various surface objects exhibit different responses and radar reflections. Additionally, SAR has limited accuracy in detecting inundation in complex settings such as vegetated and urban areas (Chini et al., 2019). To overcome this problem, we applied the InSAR Coherence method. Furthermore, we combined InSAR Coherence with the Rapid Flood Mapping method to validate the suspected flood regions.

4. Materials and methods

4.1. Study area

Our research is located in Jakarta Province (5°19′12″S–6°23′54″S and 106°22′42″E–106°58′18″E) (Fig. 1). Administratively, Jakarta borders West Java Province to the south and east, Banten Province to the west, and the Java Sea to the north. The province consists of five administrative cities: Central Jakarta, North Jakarta, West Jakarta, South Jakarta, and East Jakarta, as well as the Thousand Islands Administrative Regency. Overall, Jakarta Province has an area of 660.98 km^2 with a population of 10,672,100 people (Central Statistics Agency, 2024a, 2024b).

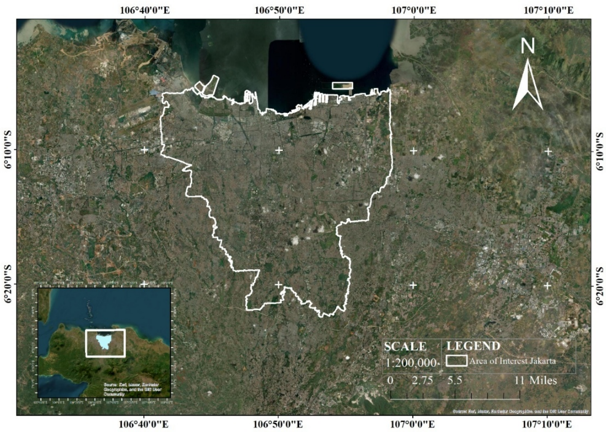

Fig. 1. Study area

4.2. Materials

4.2.1. Rainfall data

This study used rainfall data as a reference for downloading the Sentinel-1A SLC and GRD. The data was obtained from the official website of the Meteorology, Climatology, and Geophysics Agency, (https://dataonline.bmkg.go.id/home) (Table 1). The agency obtains rainfall data from manual rain gauges (observation-based), automatic rain gauges, and data from weather satellites. Also, our study refers to the Global Satellite Mapping of Precipitation (GSMaP) to visually see the rainfall area on those dates (https://sharaku.eorc.jaxa.jp/GSMaP/index.htm) (Fig. 2).

Table 1. Kemayoran meteorological station rainfall data (source: Meteorology, Climatology and Geophysics Agency, 2024)

Acquisition date	Rainfall (mm)
September 2, 2017	0
September 14, 2017	0
June 12, 2019	0
June 24, 2019	0
January 24, 2018	6.3
February 5, 2018	66
December 21, 2019	– (not available)
January 2, 2020	58.8

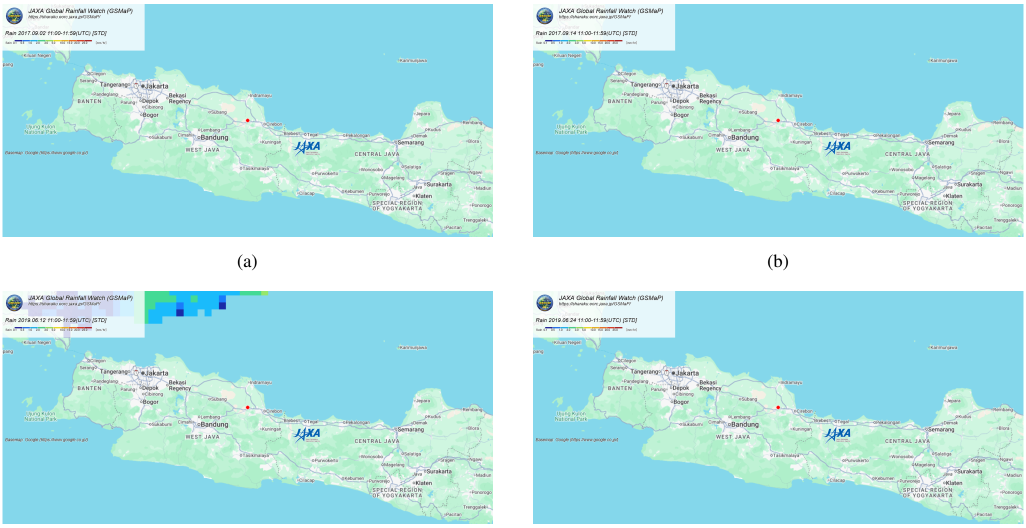

(a) (b)

(c) (d)

Rain Period

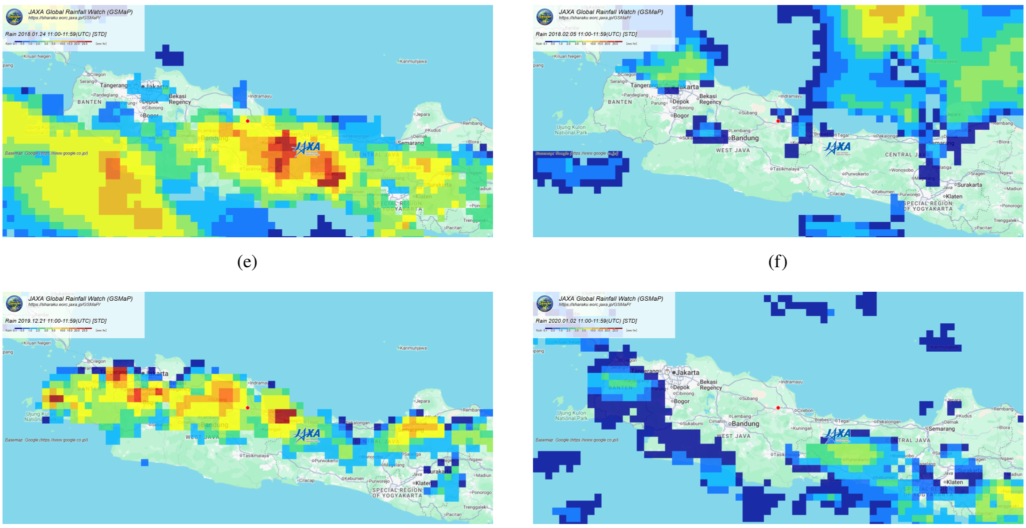

(e) (f)

(g) (h)

Fig. 2. Jakarta rainfall observation based on GSMaP: (a) September 2, 2017; (b) September 14, 2017; (c) June 12, 2019; (d) June 24, 2019; (e) January 24, 2018; (f) February 5, 2018; (g) December 21, 2019; (h) January 2, 2020 (source: Global Satellite Mapping of Precipitation (GSMaP); https://sharaku.eorc.jaxa.jp/GSMaP/index.htm)

Figure 2 shows a visualization of rainfall in Jakarta. The image shows rainfall in millimeters per hour (mm/hr). A blue color represents lower rainfall, while a red color represents higher rainfall. On dates with no rainfall, these colors will not appear.

4.2.2. Satellite imagery

Our study used Sentinel-1A with a format Single Look Complex (SLC) with a resolution (range $\times$ azi) (m) of 2.7×22 to 3.5×22 and Ground Range Detected (GRD) of 20×22. The InSAR Coherence used SLC images, while Rapid Flood Mapping (RFM) utilized GRD imagery (Table 2). Both datasets were obtained from the official ESA Copernicus (https://dataspace.copernicus.eu/).

Table 2. Sentinel-1A SLC and GRD images (source: ESA Copernicus, 2025)

Sentinel-1A image file format		Product start_stop date time (HHMMSS)		Dry/Rain	Orbit type
acquisition date	format type	SLC	GRD		
20170902	SLC and GRD	T111502_ T111530	T111503_ T111528	dry	ASC (Ascending)
20170914	SLC and GRD	T111502_ T111530	T111504_ T111529	dry	
20190612	SLC and GRD	T111510_ T111538	T111511_ T111536	dry	
20190624	SLC and GRD	T111511_ T111538	T111512_ T111537	dry	
20180124	SLC and GRD	T111500_ T111528	T111502_ T111527	rain	
20180205	SLC and GRD	T111500_ T111528	T111502_ T111527	rain	
20191221	SLC and GRD	T111515_ T111543	T111516_ T111541	rain	
20200102	SLC and GRD	T111514_ T111542	T111515_ T111540	rain	

4.2.3. Flood history data

We employed flood history data to validate the suspected flood points and analyzed the validation results. Flood history data was obtained through https://pantaubanjir.jakarta.go.id/ (Table 3). The website explains that Jakarta's flooding history results from a joint recapitulation between the Regional Disaster Management Agency (BPBD), the Meteorology, Climatology, and Geophysics Agency (BMKG), and Jakarta Opendata.

Table 3. Flood history data (source: Jakarta Provincial Government, 2020)

Time	Average water height (cm)	Inundation period (days)	Number of villages affected
September, 2017	10–80	1	2
January, 2018	5–40	1–2	25
February 2018	5–300	1–6	162
June, 2019	0	0	0
December, 2019	15–100 cm	1	41
January 2020	10–350	4	390

We also used flood history data from the Indonesian One Data Portal (https://data.go.id/) to provide more information on rainy dates, which helped identify areas affected by flooding in Jakarta (Table 4). Additionally, it was used to validate the sample points tested for flood or non-flood classifications.

Table 4. Jakarta flood history from the Indonesian One Data Portal (Ministry of National Development Planning, 2022)

Date	Number of sub-districts affected	Number of villages affected	Number of hamlet affected
September, 2 and 14 2017	0	0	0
January, 24 2018	0	0	0
February, 5 2018	11	19	65
June, 12 and 24 2019	0	0	0
December, 21 2019	0	0	0
January, 2 2020	34	143	635

The image acquisition date and flood event on January 2, 2020, indicate the highest flood impact (Table 4); however, the data from the Indonesian One Data Portal are summarized from January 1, 2020, as standing water persisted from January 1 to 2, 2020. The Indonesian One Data Portal collects historical flood data from multiple sources, including the National Disaster Management Agency (BNPB) through DIBI, regional government platforms such as Jakarta Open Data, and the Meteorology, Climatology, and Geophysics Agency (BMKG), as well as public reports from social media. In this study, historical flood data were obtained free of charge from the Jakarta Flood Monitoring and Indonesian One Data Portal websites in .xlsx format.

4.3. Methods

Flood identification using InSAR Coherence and Rapid Flood Mapping with Sentinel-1A GRD imagery is illustrated in Figure 3. Both imagery types were acquired on exact dates, with dry-period images designated as the master and rainy-period images as the slave (Fig. 3). These datasets served as the primary inputs for the subsequent processing stages. In this research, Sentinel-1A SLC imagery was processed using the InSAR Coherence method, whereas GRD imagery was analyzed through the Rapid Flood Mapping method. Both processes were conducted using SNAP software. The results display coherence values from the InSAR Coherence analysis and median backscatter values from the Rapid Flood Mapping procedure. Visualization was then performed to facilitate the validation of the suspected flood sample points. In this case, the validation process begins with determining the number of sample points (Fitzpatrick-Lins, 1981).

$$N = \frac{Z^2 pq}{E^2} \tag{1}$$

where N is the estimated sample size, p is the expected percentage accuracy, and q is $100 - p$. E is the permissible error (10%). Z is the standard normal deviate corresponding to the desired confidence level; in this study, $Z = 2$ was adopted as a conservative approximation of 1.96 for a 95% two-sided confidence level (Fitzpatrick- Lins, 1981). Our study's expected accuracy percentage (p) was 85% (Anderson et al., 1976). The acceptable tolerance limit to set an accuracy of 85% is $E \leq 10\%$ (Rosenfield et al., 1982). Therefore, the minimum number of sample points used in validating the Jakarta flood prediction is 51 sample points, which spread randomly throughout the image. Then, analyses were performed to determine the identified areas, floods, and non-floods.

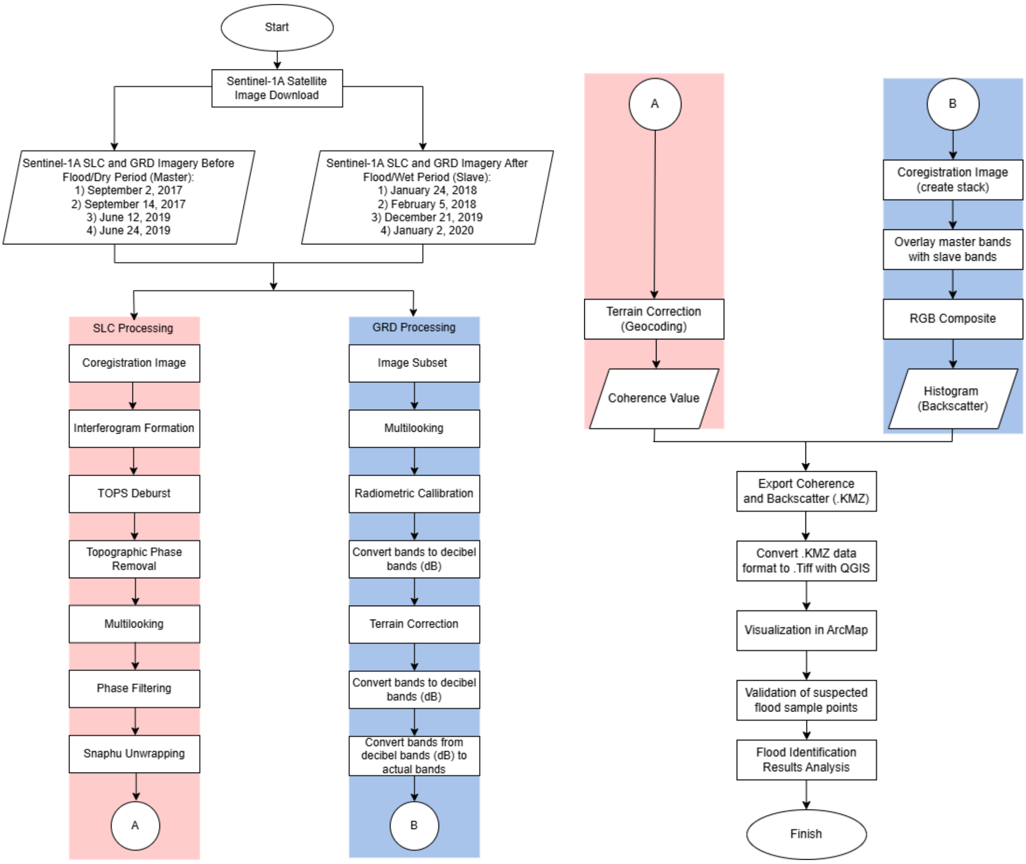

Fig. 3. Processing flow diagram

5. Results and discussion

5.1. Image acquisition period and rationale

We applied the InSAR Coherence method using Sentinel-1A SLC data, which results in a coherent image visualized in grayscale from black (low coherence) to white (high coherence). Thus, the lower the coherence can be categorized as a permanent water body or waterlogging due to flooding. On the other hand, the higher the coherence can be classified as non-permanent or non-water bodies due to flooding.

The RFM method uses Sentinel-1A GRD imagery. Previous studies (Amitrano et al., 2018; Huang and Jin, 2020; Priyatna et al., 2023; Aldiansyah et al., 2024) have demonstrated variations in this method, often combined with other techniques, although all aim to quickly and accurately map floods. We followed (Stewart, 2017), who used dry-period (pre-flood) imagery as the master and rainy-period (during-flood) imagery as the slave, allowing differentiation between flood areas and permanent water bodies. This image combination is referred to as the "dry_rain" period. The output includes an RGB composite image and backscatter decibel (dB) histogram. Because the pixel colors represent different backscatter values, the median value of this range was used for further analysis. Median values are obtained manually by examining each pixel, as their color differences impact the backscatter intensity (Fig. 5) (Stewart, 2017).

Meanwhile, previous studies that used Sentinel-1A SLC and GRD imagery (Chaabani et al., 2018; Chini et al., 2019; Huang and Jin, 2020; Papila et al., 2020; Bioresita et al., 2022; Priyatna et al., 2023) have proven that the use of periods of dry and rain can result in significant differences between areas that are flooded and those that are not. However, this study experimented with using rainy-period images for both master and slave (called the “rain_rain” period) to compare results with the “dry_rain” period and determine which combination is more effective for flood identification in Jakarta.

5.2. Evaluating “rain_rain” vs “dry_rain” image pairs for flood detection using InSAR Coherence and RFM

Sentinel-1A images were processed following the workflow in Figure 3 using different master images from the rainy and dry seasons to produce “rain_rain” and “dry_rain” results. The InSAR Coherence method generates coherence bands where each pixel’s color, ranging from black to white, represents its coherence value. Darker pixels indicate lower coherence values, identifying permanent water bodies or flooded areas, while lighter pixels show higher coherence values, representing non-flooded regions. As shown in Figure 4, solid black denotes permanent water, grayish black indicates flooded areas, and white represents non-flooded areas.

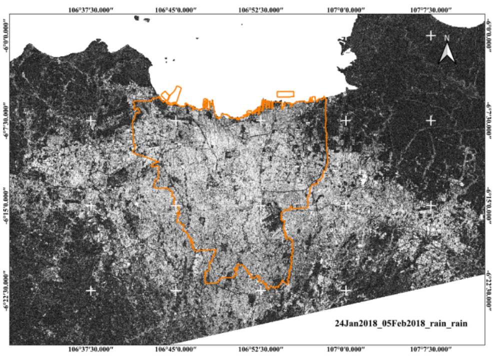

(a)

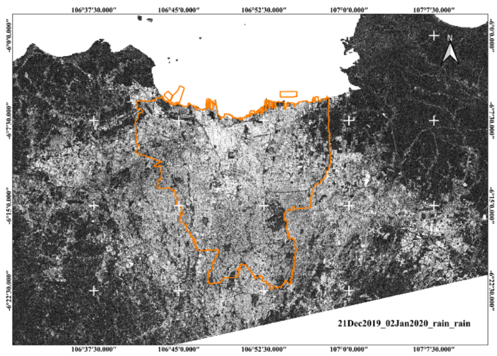

(b)

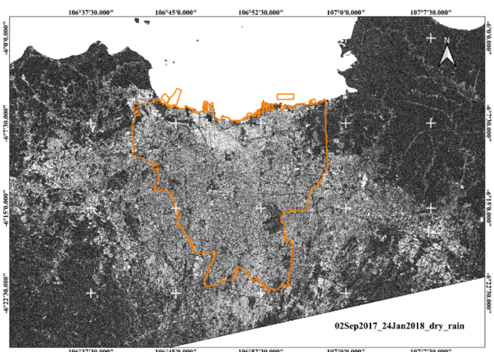

(c)

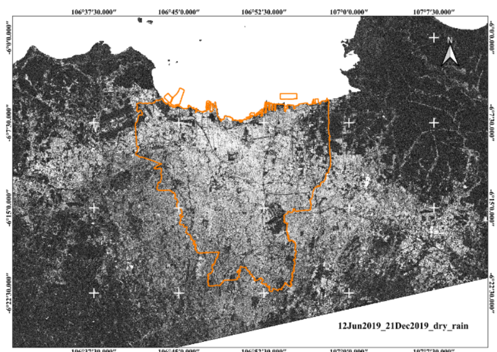

(d)

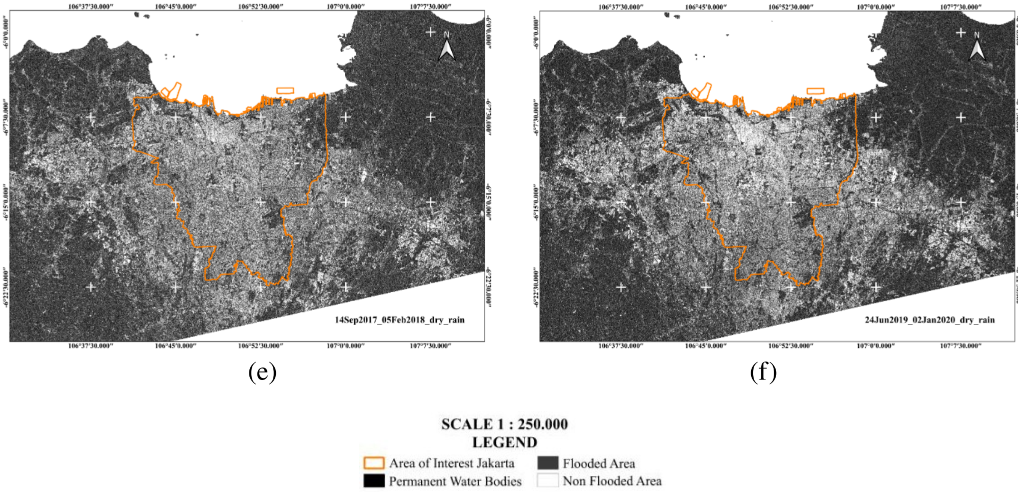

Fig. 4. The results of processing the “rain_rain” and “dry_rain” images using InSAR Coherence: (a) Coh_24Jan2018_05Feb2018_rain_rain; (b) Coh_21Dec2019_02Jan2020_rain_rain (c) Coh_02Sep2017_24Jan2018_dry_rain; (d) Coh_12Jun2019_21Dec2019_dry_rain; (e) Coh_14Sep2017_05Feb2018_dry_rain; (f) Coh_24Jun2019_02Jan2020_dry_rain

The InSAR coherence in Figure 4a and Figure 4b displays that the “rain_rain” image has bright pixel colors (white to light gray) inside Jakarta and darker pixel colors outside Jakarta, because both master and slave are acquired during the rainy period, which makes it difficult to distinguish between the regions that experienced flooding or not. Meanwhile, in the image period “dry_rain” Figures 4c–4f Jakarta’s color tends to be darker and dominated by gray. Outside Jakarta, darker color is not as concentrated as in the period of the “rain_rain” image. Therefore, using dry period imagery as master and the rainy period image as a slave present significant changes between regions that experienced flooding. The main reason is a different amplitude value between dry or rainy periods; changing master imagery between these can highly impact the result.

Meanwhile, in the Rapid Flood mapping method, the results obtained are in the form of a composite of RGB bands with different median backscatter (dB) values depending on the color of each pixel. In the composite, red represents flooding, gray represents areas that are not inundated (not flooded), black (uniform dark) represents permanent water bodies, and cyan represents certain land or land cover that is not related to flooding (not flooded) (Stewart, 2017) according to the results and legend contained in Figure 5.

Moreover, the RFM result between the “rain_rain” and “dry_rain” displays a significant color difference. In the “rain_rain” image (Fig. 5a and Fig. 5b), red dominates almost all of the image and spreads more outside Jakarta with more contrasting colors than other colors. In Jakarta, red is only visible, vague, and unclear, proving it is challenging to visually identify and interpret the Jakarta’s flood.

On the other hand, in the “dry_rain” image period (Figs. 5c–5f), red is only visible in certain areas and does not spread throughout the image. Even though the red color is located outside Jakarta, the four results of the “dry_rain” image period have a well-distributed red color (Fig. 5e and Fig. 5f) assuming widespread floods occurred in Jakarta. Meanwhile, red patch distribution can be seen in (Fig. 5c and Fig. 5d), believed to be spot floods in Jakarta. Visually, spot floods are easier to interpret than the widespread flood in the RFM because spot floods have a prominent red color in certain areas, and easily distinguished from other colors.

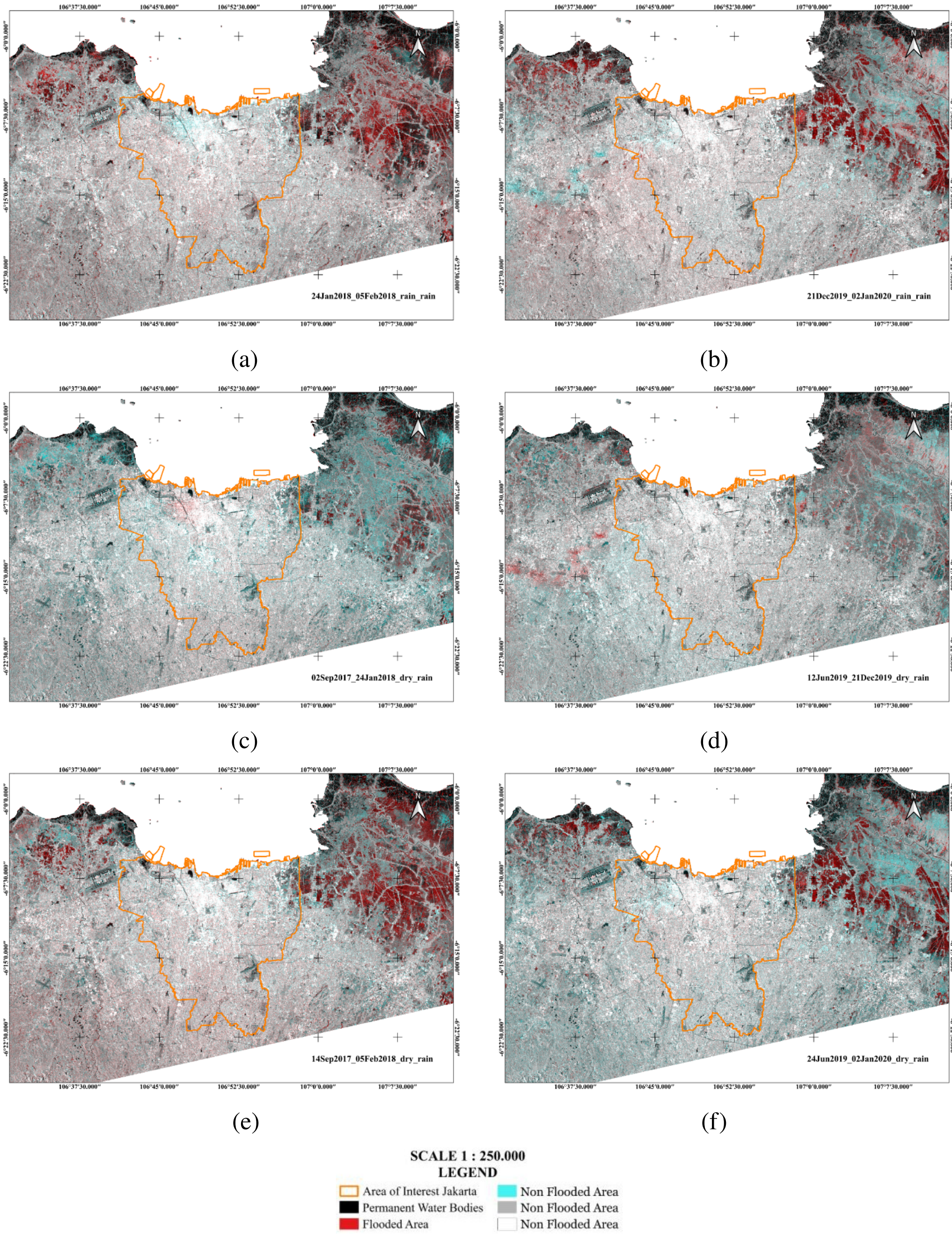

Fig. 5. The results of processing the "rain_rain" and "dry_rain" images using RFM:
(a) RGB_24Jan2018_05Feb2018_rain_rain; (b) RGB_21Dec2019_02Jan2020_rain_rain
(c) RGB_02Sep2017_24Jan2018_dry_rain; (d) RGB_12Jun2019_21Dec2019_dry_rain;
(e) RGB_14Sep2017_05Feb2018_dry_rain; (f) RGB_24Jun2019_02Jan2020_dry_rain.

Based on the results of visual analysis, it can be concluded that for both the InSAR Coherence method and Rapid Flood Mapping, the "dry_rain" image period is more effective, easier to interpret, and better at distinguishing between flooded and non-flooded areas compared to the "rain_rain" image period. Furthermore, changing the master image from a rainy season master ("rain") to a dry season master ("dry") affects the results visually (pixel color) and numerically (coherence and backscatter values). Therefore, this study uses the "dry_rain" image period. In this case, the dry-period master images used have different acquisition dates for each image pair from the 2018 and 2020 flood episodes; using the same master image across all pairs creates backscatter values that are identical across pixels in the pair, reducing variation.

5.3. Coherence value for flood

We identify Jakarta's flood using the InSAR Coherence method, resulting in values ranging from 0 to 1 (black-to-white imagery). The resulting coherence value is a statistical measure that describes the stability of interferometric signals between two SAR images taken at different times (Chini et al., 2019). In this range, a value near 1 indicates high stability or minimal change on the Earth's surface between the image acquisitions. In contrast, a value near 0 reflects significant decorrelation between the two images, indicating surface changes caused by inundation (flooding), vegetation growth, or ground movement (Refice et al., 2014; Chaabani et al., 2018; Canisius et al., 2019b; Chini et al., 2019).

Previous studies provide coherence thresholds that effectively detect floods depending on the land cover type. Floods have been identified in dense and complex urban areas at a coherence value of 0.25 (Chini et al., 2019). In urban areas near rivers or with mixed land use, the effective value is around 0.27 (Chaabani et al., 2018). Meanwhile, in rural or agricultural areas, flood detection can rely on values as low as 0.1 (Refice et al., 2014). Therefore, the coherence threshold used in this study to classify flooded and non-flooded areas – and to support analysis and validation – ranged from 0.1 to 0.27, based on Jakarta's urban and peri-urban environment.

5.4. Propose median backscatter value for flood

Every object in the Sentinel-1A GRD image has unique backscatter characteristics, which vary across land surfaces; therefore, the median value of the backscatter also varies, and the pixels in the image display various colors (Fig. 5). As a result, visual flood identification alone is insufficient to provide a robust analysis. Thus, we conducted a literature review that discussed backscatter histograms for flood identification.

In a study conducted by Martinis et al. (2018), open water surfaces produced a low backscatter coefficient due to the specular reflection of SAR signals and the high permittivity of water; thus, in VV polarization, flooded areas were identified with backscatter values ranging from –30 dB to –3 dB. In another study, floodwater in VV polarization had a backscatter range of –6 to –15 dB, where values within this interval were categorized as floodwater features (Manjusree et al., 2012). Meanwhile, the results from (Carreño Conde and De Mata Muñoz, 2019) showed that the VV polarization histogram in Zone 1 (Novillas-Pradilla de Ebro) had intensity values between –1.0 and –22 dB. The pixel backscatter values generated by Zhang et al. (2020), representing waterlogged areas, ranged between –15 and –25 dB. In contrast, (Aldiansyah et al., 2024) obtained a backscatter value of 25.54 ± 6.58 dB for the water class. Similarly, Demissie et al. (2023) reported that the backscatter value of VV polarization in floodplains was 12.45 ± 2.6 dB. Additionally, Lin et al. (2019) mapped floods by normalizing SAR intensity over time and observed backscatter values between -5 and 0 dB during flood events. Lastly, Solbø and Solheim (2005) reported a backscatter range of –16.5 to –25 dB for flooded land (water).

Based on previous research, variations in study locations led to a wide range of backscatter values (dB) for flood identification. Therefore, this study presented the reported backscatter values based on the location type – rural (Fig. 6a) and urban areas (Fig. 6b). The goal is to assist in flood identification efforts in Jakarta by providing a more explicit reference based on land characteristics.

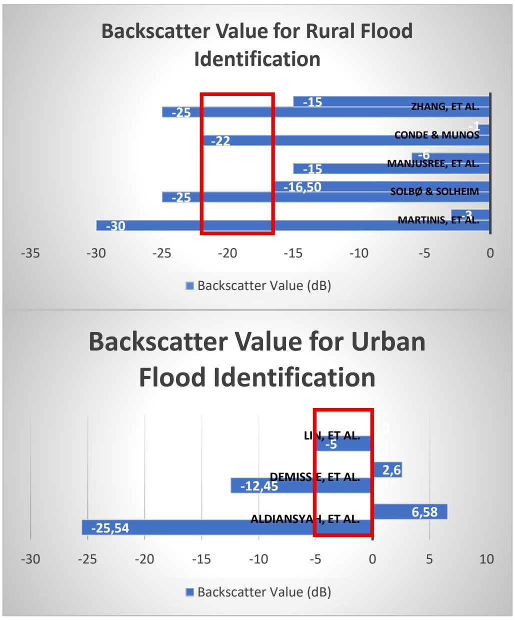

Fig. 6. Bar chart of backscatter value range (dB) from previous research for flood identification in rural (top) and urban (bottom row) areas

After being summarized, the intersecting value ranges (red boxes), resulting in a backscatter range of –16.5 dB to –22 dB for rural floods (Fig. 6a) and –5 dB to 0 dB for urban floods (Fig. 6b). These intersection ranges utilized as reference thresholds to analyze median backscatter values from the image pixels. If the median value falls within the respective range, it is categorized as flooding in rural or urban areas.

5.5. Combination of InSAR coherence and Rapid Flood Mapping to identify flood areas

5.5.1. The relation between coherence (InSAR coherence) and median backscatter (RFM)

The coherence value and the median backscatter value obtained from the InSAR Coherence and RFM methods have the same objective: to represent flood conditions in Jakarta. These two methods were analyzed visually – by interpreting the color representations from each technique – and numerically, based on literature reviews. Previous studies suggest flood-affected areas generally have a coherence value range of 0.1 to 0.27 and a median backscatter value range of –5 dB to 0 dB. Thus, the two methods are interrelated, as an area is identified and categorized as flooded when the InSAR Coherence results show dark pixels within the 0.1–0.27 range, and the Rapid Flood Mapping outputs show red pixels with a median backscatter value between –5 and 0 dB.

5.5.2. Validation of suspected flood points

The suspected flood points were validated to test the effectiveness of the InSAR Coherence and Rapid Flood Mapping (RFM) methods in identifying floods in Jakarta. In this case, validation was conducted by distributing sample points across the Jakarta area, and comparing them with a number of points located outside Jakarta. The goal was to assess the effectiveness of the InSAR Coherence and RFM methods in identifying floods using 110 sample points, consisting of 90 points in Jakarta and 20 points outside Jakarta (Fig. 7) which is higher than the minimum required sampling points in Eq. (1).

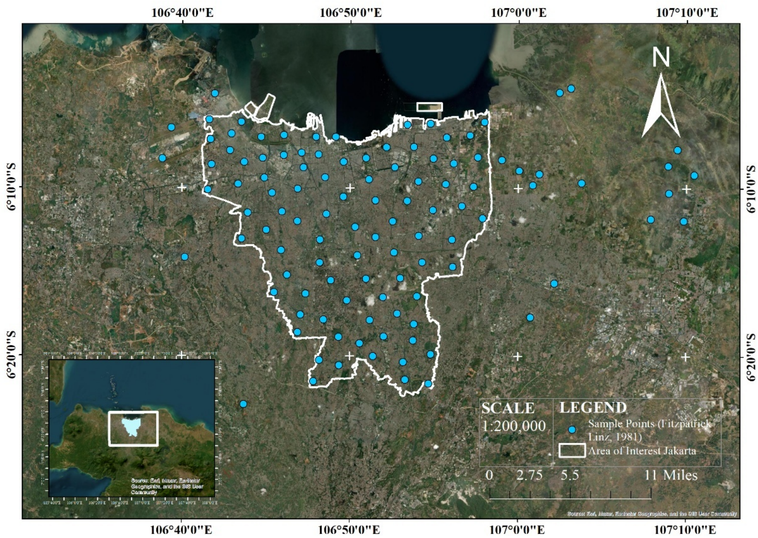

Fig. 7. Distribution of flood validation sample points in the area and outside the area of Jakarta

In the four episodes of “dry_rain” flood events, from 110 sample points only two to three sample points were identified as flooded inside and outside Jakarta (Table 5). The remaining sample points were not identified as flooded because the coherence value, median backscatter value, and pixel color did not meet the flood criteria defined by the InSAR Coherence and Rapid Flood Mapping methods (sub-section 5.3 and 5.4). In this case, the limited number of sample points identified as flooded was likely due to the random spatial distribution of the sample points, which may not have accurately captured the flooded areas.

Table 5. Identified flood points in all flood episodes, the “dry_rain” image

Flood Episode	Number of identified flood points	
	Jakarta	outside Jakarta
02Sep2017_24Jan2018_Dry_Rain	0	2
14Sep2017_05Feb2018_Dry_Rain	2	0
12Jun2019_21Dec2019_Dry_Rain	2	1
24Jun2019_02Jan2020_Dry_Rain	2	1

Meanwhile, other points outside the Jakarta area that display black and red pixels in each method are not identified as flooded because the median backscatter value is not within the range for rural or urban floods. Nonetheless, these points are vegetation or wetlands because the pixels tend to be dark, and the coherence value is low. These points have a dominant double-bounce scattering mechanism; the signal is scattered in nature (Mohammadimanesh et al., 2018b). Furthermore, vegetation areas have very low coherence values owing to the constant movement of leaves and stems (Amitrano et al., 2024).

5.5.3. Flood validation based on flood history on the Indonesian One Data portal

In the previous discussion, the randomly distributed 110 sample points could not effectively represent the areas affected by flooding. Therefore, an additional experiment was conducted by redistributing auxiliary sample points, guided by historical flood data provided by the Indonesian One Data Portal (Table 4). Table 4 shows that several sub-districts were affected at each peak flooding event in Jakarta. Therefore, we randomly distributed sample points within each flood-affected sub-district. We used the administrative boundaries of the sub-districts within Jakarta to assist in distributing sample points. A total of 11 sample points were distributed and validated for the 2018 flood episode (Fig. 8), and 34 points for the 2020 episode (Fig. 9), all within the Jakarta area. In other words, each sub- district affected by the flood is only represented by one sample point.

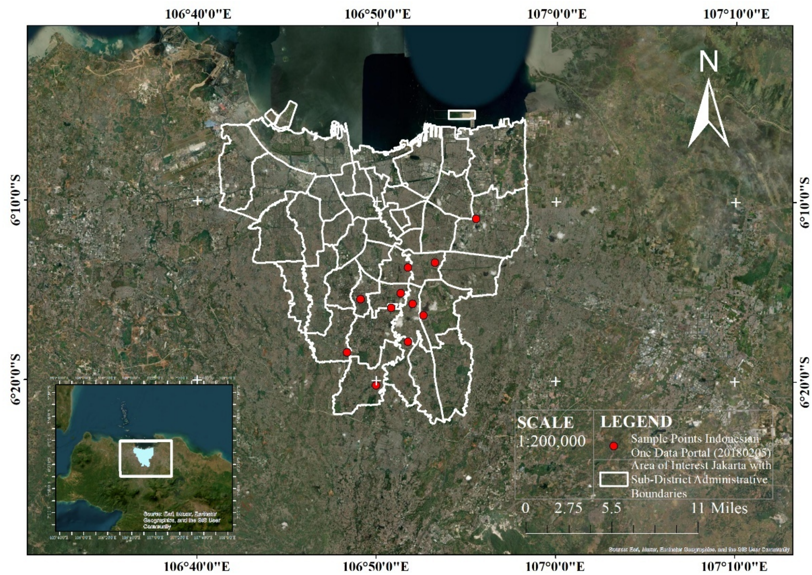

Fig. 8. Distribution of flood validation sample points in the Jakarta area during the 2018 flood episode based on the Indonesian One Data Portal

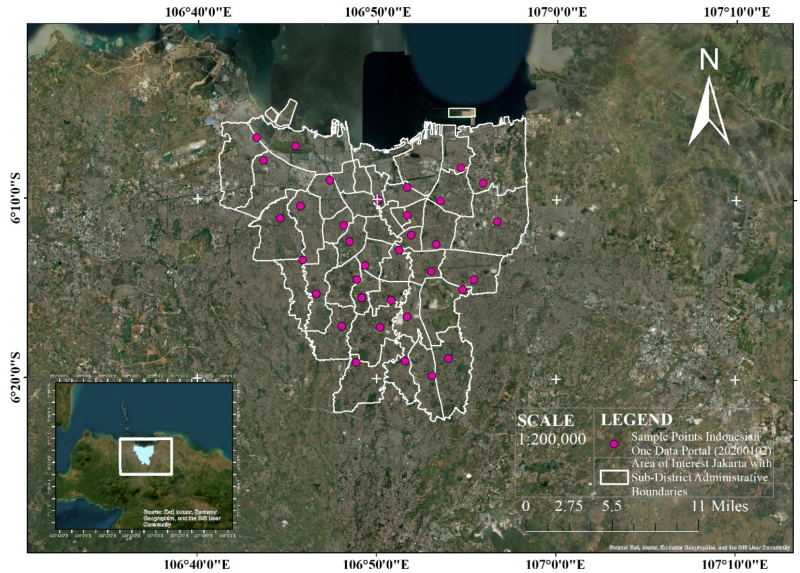

Fig. 9. Distribution of flood validation sample points in the Jakarta area during the 2020 flood episode based on the Indonesian One Data Portal

5.5.4. Flood validation of the Rapid Flood Mapping method based on flood history from the Indonesian One Data portal

In the RFM method, the “dry_rain” image periods of the 2018 and 2020 flood events were compared with the “rain_rain” periods to find out the number of points identified as flooded and to assess the effectiveness of using dry-period master images for flood identification. A total of 11 sample points were distributed and validated for the 2018 flood episode (Fig. 8), and 34 points for the 2020 episode (Fig. 9), all within the Jakarta area. The number of validation points was determined based on flood history data from the Indonesian One Data Portal, corresponding to the image acquisition dates of both flood episodes (Table 4). This review revealed no flood records for January 24, 2018, or December 21, 2019. However, significant flood events were recorded on February 5, 2018, and January 1, 2020, which are therefore considered the peak flood dates. Additionally, although only two sub-districts were reported to be flooded on January 2, 2020, the one-day gap between the peak event and the image acquisition suggests the presence of residual inundation across Jakarta.

The areas affected by the flood were within the scope of sub-districts, urban villages, and hamlet. This study determined the number of sample points based on the number of affected subdistricts. Then, the distribution of sample points was adjusted to each sub-district, with the same coordinate points between images, so that the difference between the pixel color and the median value could be seen.

The flood episodes on February 5, 2018, and January 2, 2020, successfully identified floods at all distributed sample points, as these dates correspond to the peak flood events in Jakarta (Table 6). Consequently, the pixel color and median backscatter values met the flood criteria established for the Rapid Flood Mapping method. In contrast, the January 24, 2018, and December 21, 2019, flood episodes identified flooding in only eight and 19 sub-districts, respectively. These two episodes lacked flood history records in the Indonesian One Data Portal and occurred 11 and

12 days after the peak flood dates, respectively, reducing the likelihood of widespread inundation. Nevertheless, localized flooding was still detected in some areas, supported by rainfall data from GSMaP, the Meteorology, Climatology, and Geophysics Agency, and the Jakarta Flood Monitor. Sample points not identified as flooded displayed gray or cyan pixel colors, indicating either non-inundated areas or land covers unrelated to flooding (Stewart, 2017).

Meanwhile, in the "rain_rain" flood episode, none of the sample points was classified as flooded because the tested pixels appeared gray or cyan and had median backscatter values outside the –5 dB to 0 dB range; therefore, these sub-districts were considered non-flooded land covers. Thus, the choice of the master image significantly influences the final RGB composite generated by the RFM method, as it affects pixel colour and median backscatter value at each location. This selection also impacts the effectiveness of flood detection, especially in dense urban areas such as Jakarta. Overall, the "dry_rain" combination is more reliable than "rain_rain" for visual and numerical flood identification.

Table 6. Flood validation results based on data from the Indonesian One Data Portal in the 2018 flood episode " dry_rain " compared to " rain_rain " for the Rapid Flood Mapping method

Flood Episode	Number of identified flood points
	2018
RGB_20180124_20180205_Rain_Rain	0
RGB_20170902_20180124_Dry_Rain	8
RGB_20170914_20180205_Dry_Rain	11
2020	
RGB_20191221_20200102_Rain_Rain	0
RGB_20190612_20191221_Dry_Rain	19
RGB_20190624_20200102_Dry_Rain	34

5.5.5. Flood validation of InSAR coherence method based on flood history from the Indonesian One Data Portal

We also conduct flood validation using the InSAR Coherence method, which refers to flood history data from the Indonesian One Data Portal. This ensures that the number and coordinate points of the sample locations are consistent with those used in the Rapid Flood Mapping method. This approach allows for the consistent comparison of flood identification results across methods. A total of 11 were used for the 2018 flood episode and 34 sample points for the 2020 episode. In this method, validation was conducted by comparing the coherence values of "dry_rain" and "dry_dry" image combinations to assess the differences between the dry season and periods of rainfall or flooding. Moreover, areas unaffected by floods typically retain high coherence values before and during the flood period (Chini et al., 2019). However, standing water introduces signal decorrelation in flood-affected areas, resulting in significantly lower coherence values.

In the 2018 flood episode, only one sub-district (Table 7) was identified as flooded: Jatinegara (row 1 in Table 9). In the 2019 episode, Tebet was the only sub-district (Table 7) detected as flooded (row 2 in Table 9). For the 2020 flood, seven sub-districts (Table 7) were identified: Kalideres (row 3 in Table 9), Jagakarsa (row 4 in Table 9), Pasar Minggu (row 5 in Table 9), Tebet (row 6 in Table 9), Jatinegara (row 7 in Table 9), Makasar (row 8 in Table 9), and Cengkareng (row 9 in Table 9). These areas were categorized as flooded because their coherence values significantly dropped – from near 1.0 during the dry season to 0.1–0.27 at the flood peak. This drop indicates pixel-level changes at each validated sample point, consistent with flood presence. However, not all coherence values decrease, indicating flooding. In the 2018 episode, four sub-districts, and in the 2020 episode, 18 sub-districts showed a decline in coherence but were not classified as flooded, as their values did not fall within the flood threshold range of 0.1 to 0.27.

Table 7. Flood validation results based on data from the Indonesian One Data Portal in the 2018, 2019, 2020 flood episode for the InSAR Coherence method

Flood Episode	Number of identified flood points
2018	1
2019	1
2020	7

The other points were not included in the flood category because of several anomalies. The first anomaly was the decrease in the coherence value from the dry to the rainy period, resulting in a lower coherence value than the peak of the flood. The coherence value should be lower when the peak of the flood occurs because the rainfall is high; therefore, the water stagnates longer. Second, there are points/sub-districts whose coherence values tend to be stable, and there have been no significant changes during the dry period or the peak of the flood; the pixels have low coherence values or are in stable conditions; therefore, these points are categorized as not flooded because they do not experience significant changes from the dry and rainy periods to the peak of the flood. According to data from the Indonesian One Data Portal (Table 4), the validated sub-districts experienced flooding on February 5, 2018, and January 2, 2018, so the coherence value should be 0.1 to 0.27. However, the validation results identified floods in only one sub-district in the 2018 and 2019 flood episodes and seven sub-districts in the 2020 flood episode because each sub-district is only represented by one sample point, while in one sub-district, there are undoubtedly several villages and hamlet. Thus, the sample points identified as not flooded are located in villages or hamlet that are not flooded. Overall, the validated images experienced significant changes in display Figure 10. In the dry season (Fig. 10a and Fig. 10d), the image color tends to be brighter and dominated by white pixels, whereas in the rainy season (Fig. 10b and Fig. 10e) and peak floods (Fig. 10c and Fig. 10f), the image color tends to be darker and dominated by gray or black pixels. This is due to changes and decreases in coherence values caused by flooding, resulting in the coherence value approaching 1 changing to the coherence value approaching 0. Therefore, the placement of sample points significantly affects the results of Jakarta flood identification.

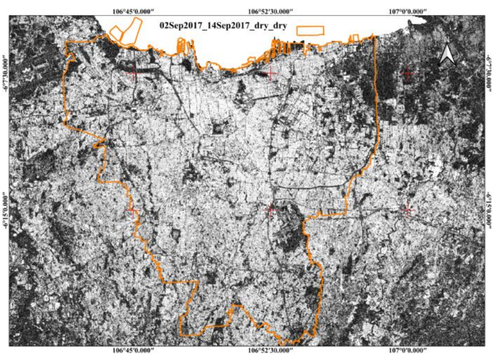

(a)

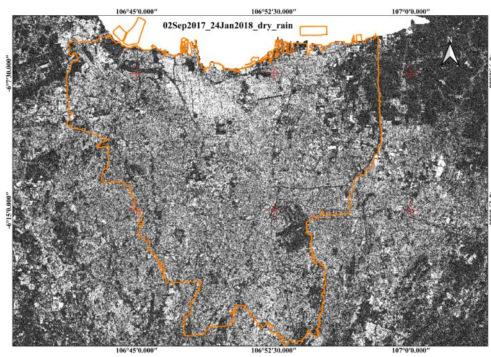

(b)

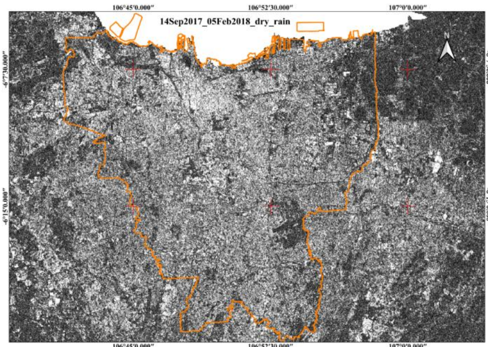

(c)

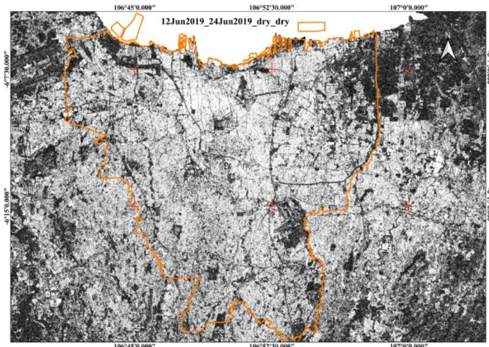

(d)

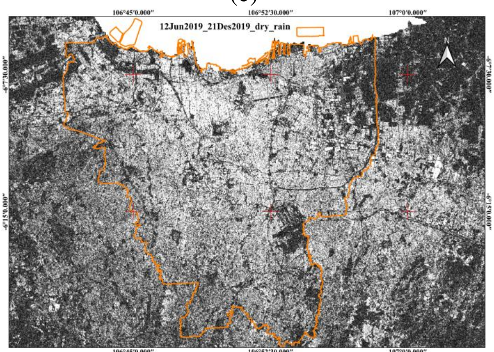

(e)

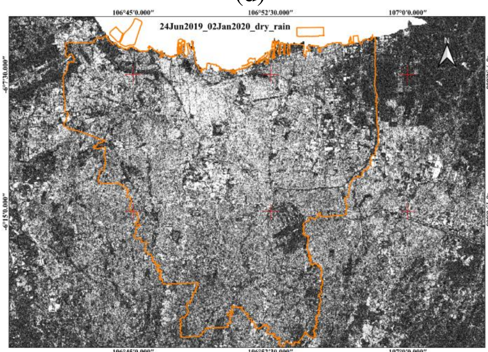

(f)

Fig. 10. Comparison of the "dry_dry" and "dry_rain" image periods in the InSAR Coherence method: (a) Coh_02Sep2017_14Sep2017_dry_dry; (b) Coh_02Sep2017_24Jan2018_dry_rain; (c) Coh_14Sep2017_05Feb2018_dry_rain; (d) Coh_12Jun2019_24Jun2019_dry_dry; (e) Coh_12Jun2019_21Dec2019_dry_rain; (f) Coh_24Jun2019_02Jan2020_dry_rain

5.5.6. Flood identification validation based on InSAR coherence and Rapid Flood Mapping method

Flood validation using InSAR Coherence (Table 7) and Rapid Flood Mapping (Table 6) methods obtained different identification results; several sample points (in sub-districts) were only identified as flooded using one method. Then, a re-check was carried out on the flood identification results obtained in the InSAR Coherence and Rapid Flood Mapping methods, namely validation points that fall into the flood criteria in both methods, with coherence values in the range of 0.1–0.27 and median backscatter values between –5 and 0 dB were concluded as floods. In contrast, points that only fall into the flood criteria in one of the methods were concluded as not floods, so we summarize the validation results in Table 8. Table 8 shows that on January 24, 2018, during flood episodes, no points were identified as flooded from 11 sample points using either the InSAR Coherence or Rapid Flood Mapping methods because no points met the flood criteria for either method. This was likely due to the low rainfall during the episode, which was only 6.3 mm. Additionally, the validated sample points refer to historical flood data that occurred on February 5, 2018; therefore, the time difference was quite long.

Table 8. Final results of flood identification validation on InSAR Coherence and Rapid Flood Mapping methods for each flood episode

Flood Episode	Number of identified flood points using the InSAR Coherence and Rapid Flood Mapping methods	Total sample points
02Sep2017_24Jan2018_Dry_Rain	0	11
14Sep2017_05Feb2018_Dry_Rain	1	11
12Jun2019_21Dec2019_Dry_Rain	1	34
24Jun2019_02Jan2020_Dry_Rain	7	34

In the February 5, 2018, flood episode, only one sample point was identified as flooded (Jatinegara) (row 1 in Table 9) from 11 sample points. In addition, the December 21, 2019, flood episode also resulted in one point being identified as flooded (Tebet) (row 2 in Table 9) from 34 sample points. These two sub-districts met the flood criteria for the InSAR Coherence and Rapid Flood Mapping methods.

On January 2, 2020, during another flood episode, seven sample points were identified as flooded from 34 sample points and met the flood criteria for both methods. The seven sub-districts were Kalideres, Jagakarsa, Pasar Minggu, Tebet, Jatinegara, Makasar, and Cengkareng (rows 3–9 in Table 9). In the InSAR Coherence method, all seven points showed a significant decrease in coherence values from the dry to the rainy season and further to the peak of the flood.

Table 9. Inter comparison between: InSAR Coherence and Rapid Flood Mapping. Visualization from Google Earth Pro is also presented

Subdistrict	InSAR Coherence	Rapid Flood Mapping	Google Earth Pro View
14Sep2017_05Feb2018_Dry_Rain			
Jatinegara 106°53'12.704"E 6°13'24.556"S	 0.24755 coherence	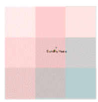 Median: –3.3862683773040771	
12Jun2019_21Dec2019_Dry_Rain			
Tebet 106°51'13.129"E 6°12'50.322"S	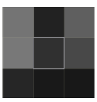 0.24866 coherence	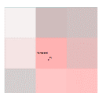 Median: –0.455684036016464231	
24Jun2019_02Jan2020_Dry_Rain			
Kalideres 106°43'14.698"E 6°6'35.152"S	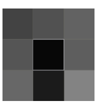 0.15015 coherence	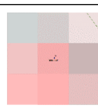 Median: –2.21662902832031251	

Table continued on the next page

Table 10. Inter comparison between: InSAR Coherence and Rapid Flood Mapping. Visualization from Google Earth Pro is also presented

Table continued from the previous page

Subdistrict	InSAR Coherence	Rapid Flood Mapping	Google Earth Pro View
14Sep2017_05Feb2018_Dry_Rain			
Jagakarsa 106°48’50.414"E 6°19’6.227"S	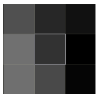 0.24320 coherence	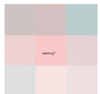 Median: –2.1455733776092531	
Pasar Minggu 106°50’9.902"E 6°17’7.499"S	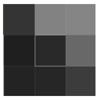 0.22417 coherence	 Median: –1.80374979972839361	
Tebet 106°51’13.129"E 6°12’50.322"S	 0.15916 coherence	 Median: –2.10857558250427251	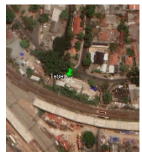
Jatinegara 106°53’0.653"E 6°14’1.566"S	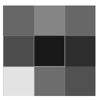 0.18769 coherence	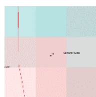 Median: –2.8835759162902831	
Makasar 106°54’44.558"E 6°15’1.299"S	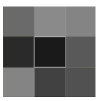 0.19137 coherence	 Median: –4.3671422004699711	
Cengkareng 106°43’38.147"E 6°7’51.644"S	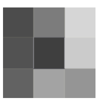 0.27100 coherence	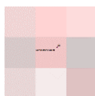 Median: –2.70062112808227541	

On the other hand, the sample points categorized as non-flooded did not meet criteria in either method. Some were flooded in Rapid Flood Mapping but not in InSAR Coherence (no significant coherence drop). Thus, integrated validation found few flooded sub-district points.

Three main factors influenced the results. First, rainfall magnitude on image-acquisition date: scenes captured near the flood peak (high rainfall) yielded more flooded points than taken during lower rainfall. Second, sample-point placement: points were distributed on sub-district boundaries from the One Data Indonesia Portal, but sub-district – containing several villages/hamlets – had only one sample point. The second limitation in this study’s validation is the pixel size – 28 m × 22 m for SLC and 30 m × 30 m for GRD – making a single pixel insufficient to represent an entire flood- affected sub-district. Misplacement lowers accuracy since one SLC/GRD pixel cannot represent an entire sub-district. Third, flood extent: inundation rarely covers entire sub-districts, usually only some villages/hamlets. Thus, points in non-inundated areas were labelled "not flooded" though other parts were underwater. Despite these limits, integrating InSAR Coherence and Rapid Flood Mapping was effective for detecting floods in dense urban areas like Jakarta, and each can cross-validate the other.

6. Results and discussion

Our study shows that the "dry_rain" period is more effective than "rain_rain" for identifying floods in Jakarta, as InSAR Coherence maps and RGB composites from Rapid Flood Mapping show clearer color changes and greater coherence/backscatter variation, improving visual and numerical flood identification. InSAR Coherence and Rapid Flood Mapping complement each other for urban flood detection, with integration enhancing accuracy through mutual validation.

Nonetheless, several factors influence the outcomes of this integration. High rainfall at image capture increases detected floods compared to low- rainfall scenes. Identification is also affected by point placement and flood extent. Each sample point represents a sub-district, but one pixel (SLC: 28 × 22 m, GRD: 30 × 30 m) cannot represent the whole area. Flooding is often localized, so sample points may be located in areas not inundated, even if other parts of the sub-district experienced flooding.

Based on this study's limitations, several suggestions are proposed for future research: using higher-resolution imagery; comparing InSAR Coherence and Rapid Flood Mapping with other techniques, such as machine learning, to assess their strengths and weaknesses; and expanding reliability analysis by creating "uncertainty maps" to indicate result accuracy. For those continuing this research with the same methods, flood validation should involve distributing sample points across smaller areas to represent flooded zones better. Validation can also use additional reference data, such as flood history from the Satu Data Indonesia Portal, with points placed at finer spatial levels (e.g., RW or RT) and supported by sample points with clearly defined statuses, inundated or non-inundated, then verify them using both methods.

Author contributions

Conceptualization: L.L., N.S.; data curation L.L.; methodology: N.S.; processing data: L.L.; formal analysis: L.L.; .visualization: L.L.; writing - original draft and editing: L.L., N.S.; supervision: N.S.

Data availability statement

The data used in this study were downloaded from the official websites of ESA Copernicus, the Meteorology, Climatology, and Geophysics Agency (BMKG), the Jakarta Flood Monitoring Agency, and the Indonesian One Data Portal. The websites are listed and explained in section 4.2 of the Materials section. The results of this study are available from the corresponding authors upon request via e-mail).

Acknowledgements

This research received no specific grant from any funding agency in the public, commercial, or not-for-profit sectors. The Sentinel-1A Single Look Complex and Ground Range Detected data used in this study were obtained from the European Space Agency Copernicus. The authors thank the anonymous reviewers for their valuable time and insightful feedback.

References

Abidin, H. ., Andreas, H., Gumilar, I. et al. (2015). Study on the risk and impacts of land subsidence in Jakarta. *Proc. Int. Assoc. Hydro.Sci.*, 372, 115–120. doi: 10.5194/piahs-372-115-2015.

Aldiansyah, S., Saputra, R.A., Wahid, K.A. et al. (2024). Rapid Flood Inundation Mapping Using Multi-Temporal Sentinel-1 SAR: An Example from Kendari City. *J. Geosains Dan Remote Sens*. doi: 10.23960/jgrs.ft.unila.205.

Amitrano, D., Di Martino, G., Iodice, A. et al. (2018). Unsupervised Rapid Flood Mapping Using Sentinel-1 GRD SAR Images. *IEEE Trans. Geosci. Remote Sens.*, 56(6), 3290–3299. doi: 10.1109/TGRS.2018.2797536.

Amitrano, D., Di Martino, G., Di Simone, A. et al. (2024). Flood Detection with SAR: A Review of Techniques and Datasets. *Remote Sens.*, 16(4), 656. doi: 10.3390/rs16040656.

Anderson, J.R., Hardy, E.E., Roach, J.T. et al. (1976). A Land Use and Land Cover Classification System for Use with Remote Sensor Data.

Bioresita, F., Hayati, N., Ngurawan, M.G.R. et al. (2022). INTEGRATING INSAR COHERENCE AND BACKSCATTERING FOR IDENTIFICATION OF TEMPORARY SURFACE WATER, CASE STUDY: SOUTH KALIMANTAN FLOODING, INDONESIA. *Int. Arch. Photogr. Remote Sens. Spatial Inf. Sci.*, XLIII-B3-2022, 33–39. doi: 10.5194/isprs-archives- XLIII-B3-2022-33-2022.

Brisco, B., Ahern, F., Murnaghan, K. et al. (2017). Seasonal Change in Wetland Coherence as an Aid to Wetland Monitoring. *Remote Sens.*, 9(2), 158. doi: 10.3390/rs9020158.

Canisius, F., Brisco, B., Murnaghan, K. et al. (2019a). SAR Backscatter and InSAR Coherence for Monitoring Wetland Extent, Flood Pulse and Vegetation: A Study of the Amazon Lowland. *Remote Sens.*, 11(6), 720. doi: 10.3390/rs11060720.

Canisius, F., Brisco, B., Murnaghan, K. et al. (2019b). SAR Backscatter and InSAR Coherence for Monitoring Wetland Extent, Flood Pulse and Vegetation: A Study of the Amazon Lowland. *Remote Sens.*, 11(6), 720. doi: 10.3390/rs11060720.

Carreño Conde, F., and De Mata Muñoz, M. (2019). Flood Monitoring Based on the Study of Sentinel-1 SAR Images: The Ebro River Case Study. *Water*, 11(12), 2454. doi: 10.3390/w11122454.

Cartus, O., Santoro, M., Wegmuller, U. et al. (2022). Sentinel-1 Coherence for Mapping Above-Ground Biomass in Semiarid Forest Areas. *IEEE Geosci. Remote Sens. Lett.*, 19, 1–5. doi: 10.1109/LGRS.2021.3071949.

Central Statistics Agency. (2024a). Area by Regency/City. Retrieved August, 2025, from https://jakarta.bps.go.id/id/statistics-table/2/MzgjMg==/luas-daerah-menurut-kabupaten-kota.html.

Central Statistics Agency. (2024b). Population by Regency/City in Jakarta Province (People), 2023. Retrieved August, 2025, from https://jakarta.bps.go.id/id/statistics-table/2/MTI3MCMy/jumlah-penduduk-menurut-kabupaten-kota-di-provinsi-dki-jakarta-.html.

Chaabani, C., Chini, M., Abdelfattah, R. et al. (2018). Flood Mapping in a Complex Environment Using Bistatic TanDEM-X/TerraSAR-X InSAR Coherence. *Remote Sens.*, 10(12), 1873. doi: 10.3390/rs10121873.

Chini, M., Pelich, R., Pulvirenti, L. et al. (2019). Sentinel-1 InSAR Coherence to Detect Floodwater in Urban Areas: Houston and Hurricane Harvey as A Test Case. *Remote Sens.*, 11(2), 107. doi: 10.3390/rs11020107.

Ciecholewski, M. (2017). River channel segmentation in polarimetric SAR images: Watershed transform combined with average contrast maximisation. *Expert Syst. Application,* 82, 196–215. doi: 10.1016/j.eswa.2017.04.018.

DeLancey, E.R., Brisco, B., Canisius, F. et al. (2019). The Synergistic Use of RADARSAT-2 Ascending and Descending Images to Improve Surface Water Detection Accuracy in Alberta, Canada. *Canadian J. Remote Sens.*, 45(6), 759–769. doi: 10.1080/07038992.2019.1691516.

Demissie, B., Vanhuysse, S., Grippa, T. et al. (2023). Using Sentinel-1 and Google Earth Engine cloud computing for detecting historical flood hazards in tropical urban regions: A case of Dar es Salaam. *Geomat. Nat. Hazards Risk*, 14(1), 2202296. doi: 10.1080/19475705.2023.2202296.

Dwi, A., and Nurhadi. (2022). Ini 10 Banjir Terparah di Jakarta Sepanjang Sejarah. TEMPO. Retrieved August, 2025, from https://www.tempo.co/arsip/ini-10-banjir-terparah-di-jakarta-sepanjang-sejarah-271922.

ESA Copernicus. (2025). Sentinel-1 Products. Retrieved August, 2025, from https://sentiwiki.copernicus.eu/web/s1-products.

Fitzpatrick-Lins, K. (1981). *Comparison of Sampling Procedures and Data Analysis for a Land-Use and Land-Cover Map*. PHOTOGRAMMETRIC ENGINEERING.

Garg, S., Dasgupta, A., Motagh, M. et al. (2024). Unlocking the full potential of Sentinel-1 for flood detection in arid regions. *Remote Sens. Environ.*, 315, 114417. doi: 10.1016/j.rse.2024.114417.

Huang, M., and Jin, S. (2020). Rapid Flood Mapping and Evaluation with a Supervised Classifier and Change Detection in Shouguang Using Sentinel-1 SAR and Sentinel-2 Optical Data. *Remote Sens.,* 12(13), 2073. doi: 10.3390/rs12132073.

Jakarta Provincial Government. (2020). Cross- Year Flood Data. Retrieved August, 2025, from https://pantaubanjir.jakarta.go.id/data-banjir-lintas-tahun.

Kodoatie, R.J. (2013). Rekayasa dan Manajemen Banjir Kota. Penerbit ANDI. Retrieved August, 2025, from https://books.google.co.id/books?hl=id&lr=&id=-jMhEAAAQBAJ&oi=fnd&pg=PP1&dq=Rekayasa+dan+manajemen+banjir+kota&ots=dUx1YcNSL_&sig=QwloqjZb6GPTa-fwTgrayuPPCZ4&redir_esc=y#v=onepage&q&f=false.

Lin, Y. N., Yun, S.-H., Bhardwaj, A. et al. (2019). Urban Flood Detection with Sentinel-1 Multi-Temporal Synthetic Aperture Radar (SAR) Observations in a Bayesian Framework: A Case Study for Hurricane Matthew. *Remote Sens.*, 11(15), 1778. doi: 10.3390/rs11151778.

Manjusree, P., Prasanna Kumar, L., Bhatt, C.M. et al. (2012). Optimization of threshold ranges for rapid flood inundation mapping by evaluating backscatter profiles of high incidence angle SAR images. *Int. J. Disaster Risk Sci.*, 3(2), 113–122. doi: 10.1007/s13753-012-0011-5.

Mantra, I.B. (2003). *Demografi Umum. Pustaka Pelajar Edisi 2, Bab 2*. Retrieved August, 2025, from https://lccn.loc.gov/2003530255.

Martinis, S., Plank, S., and Cwik, K. (2018). The Use of Sentinel-1 Time-Series Data to Improve Flood Monitoring in Arid Areas. *Remote Sens.*, 10(4), 583. doi: 10.3390/rs10040583.

Meteorology, Climatology and Geophysics Agency. (2024). Daily Climate Data. Retrieved August, 2025, from https://dataonline.bmkg.go.id/data-harian.

Ministry of National Development Planning. (2022). Flood Disaster Incident Data in DKI Jakarta – Dataset. Retrieved August, 2025, from https://data.go.id/dataset?q=Banjir+DKI.

Mohammadimanesh, F., Salehi, B., Mahdianpari, M. et al. (2018a). Multi-temporal, multi-frequency, and multi-polarization coherence and SAR backscatter analysis of wetlands. ISPRS Journal of Photogrammetry and Remote Sensing, 142, 78–93. doi: 10.1016/j.isprsjprs.2018.05.009.

Mohammadimanesh, F., Salehi, B., Mahdianpari, M. et al. (2018b). Wetland Water Level Monitoring Using Interferometric Synthetic Aperture Radar (InSAR): A Review. *Canadian J. Remote Sens.*, 44(4), 247–262. doi: 10.1080/07038992.2018.1477680.

Papila, I., Alganci, U., and Sertel, E. (2020). Sentinel-1 based flood mapping using interferometric coherence and intensity change detection approach. *Int. Arch. Photogr. Remote Sens. Spatial Inf. Sci.*, XLIII-B3-2020, 1697–1703. doi: 10.5194/isprs-archives- XLIII-B3-2020-1697-2020.

Pasaribu, J.M., Prasasti, I., and Sofan, P. (2015). *Penurunan muka tanah dan hubungannya dengan daerah rawan banjir di Jakarta*. In Pemanfaatan Penginderaan Jauh untuk Mitigasi Bencana Banjir. IPB Press.

Pierdicca, N., Pulvirenti, L., and Chini, M. (2018). *Flood Mapping in Vegetated and Urban Areas and Other Challenges: Models and Methods*. In A. Refice, A. D'Addabbo, and D. Capolongo (Eds.), Flood Monitoring through Remote Sensing (pp. 135–179). Springer International Publishing. doi: 10.1007/978-3-319-63959-8_7.

Priyatna, M., Khomarudin, M. R., Wijaya, S. K. et al. (2023). Rapid Flood Mapping Using Statistical Sampling Threshold Based on Sentinel-1 Imagery in the Barito Watershed, South Kalimantan Province, Indonesia. *J. Eng. Technological Sci.*, 55(1), 98–107. doi: 10.5614/j.eng.technol.sci.2023.55.1.10.

Pulvirenti, L., Chini, M., Pierdicca, N., and Boni, G. (2016). Use of SAR Data for Detecting Floodwater in Urban and Agricultural Areas: The Role of the Interferometric Coherence. *IEEE Trans. Geosci. Remote Sens.*, 54(3), 1532–1544. doi: 10.1109/TGRS.2015.2482001.

Refice, A., Capolongo, D., Pasquariello, G. et al. (2014). SAR and InSAR for Flood Monitoring: Examples With COSMO-SkyMed Data. *IEEE J. Selected Topics in Appl. Earth Obs. Remote Sens.*, 7(7), 2711–2722. doi: 10.1109/JSTARS.2014.2305165.

Riyanto, I., Rizkinia, M., Arief, R. et al. (2022). Three-Dimensional Convolutional Neural Network on Multi-Temporal Synthetic Aperture Radar Images for Urban Flood Potential Mapping in Jakarta. *Appl. Sci.*, 12(3), 1679. doi: 10.3390/app12031679.

Rosenfield, G.H., Fitzpatrick, K., and Ling, H.S. (1982). Sampling for The Thematic Map Accuracy Testing. *Photogr. Eng. Remote Sens.*, 48, 131–137.

Santoro, M., Askne, J.I.H., Wegmuller, U. et al. (2007). Observations, Modeling, and Applications of ERS-ENVISAT Coherence Over Land Surfaces. *IEEE Trans. Geosci. Remote Sens.*, 45(8), 2600–2611. doi: 10.1109/TGRS.2007.897420.

Santoro, M., Wegmuller, U., and Askne, J.I.H. (2010). Signatures of ERS-Envisat Interferometric SAR Coherence and Phase of Short Vegetation: An Analysis in the Case of Maize Fields. *IEEE Trans. Geosci. Remote Sens.*, 48(4), 1702–1713. doi: 10.1109/TGRS.2009.2034257.

Schumann, G., Giustarini, L., Tarpanelli, A. et al. (2023). Flood Modeling and Prediction Using Earth Observation Data. *Surv. Geophys.*, 44(5), 1553–1578. doi: 10.1007/s10712-022-09751-y.

Selmi, S., Ben Abdallah, W., and Abdelfatteh, R. (2014). Flood Mapping Using InSAR Coherence Map. *Int. Arch. Photogr. Remote Sens. Spatial Inf. Sci.*, XL-7, 161–164. doi: 10.5194/isprsarchives- XL-7-161-2014.

Solbø, S., and Solheim, I. (2005). Towards operational flood mapping with satellite SAR.

Stewart, Dr.C. (2017). ESA Echoes in Space- Hazard: Flood mapping with Sentinel-1 [Video recording]. EO College. Retrieved August, 2025, from https://www.youtube.com/watch?v=derOXkPCH80.

Tay, C.W.J., Yun, S.-H., Chin, S.T. et al. (2020). Rapid flood and damage mapping using synthetic aperture radar in response to Typhoon Hagibis, Japan. *Scientific Data*, 7(1), 100. doi: 10.1038/s41597-020-0443-5.

Twele, A., Cao, W., Plank, S. et al. (2016). Sentinel-1-based flood mapping: A fully automated processing chain. *Int. J. Remote Sens.* 37(13), 2990–3004. doi: 10.1080/01431161.2016.1192304.

Zhang, M., Chen, F., Liang, D. et al. (2020). Use of Sentinel-1 GRD SAR Images to Delineate Flood Extent in Pakistan. *Sustainability*, 12(14), 5784. doi: 10.3390/su12145784.